Batteries & Supercaps

Research Article
doi.org/10.1002/batt.202400065

Chemistry Europe
European Chemical Societies Publishing

www.batteries-supercaps.org

Surface Nitriding Enables Improved Intercalation Pseudocapacitance of T–Nb2O5 for Lithium-Ion Batteries

Wei Fang,[a] Lingling Zhang,*[b] Ming Yang,[c] Hongyuan Zhang,[a] Lina Wu,[a] Enjie Dong,[a] Xiangjun Xiao,[c] Yan Zhang,[c] Shuaifeng Lou,[c] and Geping Yin*[a, c]

The low electrical conductivity limits the application of T–Nb_2O_5 as anode materials for practical applications. The large-grain T–Nb_2O_5 nanowires with nitrogen doping are obtained by simple hydrothermal and annealing treatments. After nitriding with ammonia, an amorphous layer of NbON as an intermediate is formed and then the new crystalline NbN is generated with the deepening of the nitriding degree, causing homogeneous pores on the surface of the T–Nb_2O_5 and thus increasing the specific surface area. Meanwhile, the formation of the nitriding layer enhances the electrical conductivity, inducing a pseudocapacitance mechanism. Therefore, the N–T–Nb_2O_5 nanowire demonstrates superior electrochemical performance. Specifically, the 45N–T–Nb_2O_5 nanowires delivered a first reversible specific capacity of 238.33 mAh g^{-1} at 0.1 C, higher than of theoretical capacity (201.6 mAh g^{-1}). However, the excessive nitride will be completely converted into NbN, reducing the initial lithium storage of the material due to the lack of a lithium storage site, which has not been previously discussed. Besides, at the high rate of 100 C, with the deepening of nitride degree of the T–Nb_2O_5, the higher the rate performance. Therefore, to find the balance between the high rate performance and the initial lithium storage amount, the nitride degree should be strictly controlled.

1. Introduction

Owing to continuously increased greenhouse gas emissions and the advantages of lithium-ion batteries (LIBs), there is an urgent need to develop and implement electric vehicles (EVs) powered by LIBs. The EVs have high requirements to improve the safety, energy density, and power density of LIBs.[1–4] The orthorhombic niobium oxide (T–Nb_2O_5) has a superior safety lithium-intercalated potential of among 1.0~2.0 V (*vs* Li^+/Li), which can avoid safety concerns, including electrolyte reduction, solid/electrolyte interface (SEI) film, and lithium dendrite growth issue.[5–7] Besides, the multivalent chemistry in T–Nb_2O_5 exhibits multiple redox reactions (Nb^{5+}/Nb^{4+} and Nb^{4+}/Nb^{3+}), providing better store capacity.[8–10] Meanwhile, its orthogonal T–Nb_2O_5 with considerable interlayer distance (0.39 nm) is a typical intrinsic insertion-type pseudocapacitance capacitor material, with good high rate performance and cycle stability, which is expected to achieve high power electrochemical energy storage.[11–13] Despite these advantages, the poor electrical conductivity of T–Nb_2O_5 (ca.3×10^{-6} S cm^{-1}) seriously limits its high rate capacity, further hampering its practical applications.[14–16]

Tremendous efforts have been devoted to improving the conductivity of T–Nb_2O_5 material. Since the microstructure facilitates the exertion of its pseudo-capacitive characteristics, nanostructure, such as (nanospheres,[17–19] nanosheets,[20] and nanowires,[21,22] is designed to achieve the maximum amount of lithium intercalated in material and exerts effective pseudocapacitance effect. Notably, one-dimensional large-grain micro-nanomaterials with a high aspect ratio can effectively avoid some nanomaterial issues, i.e. poor crystallization, small volume and energy density, and largely irreversible capacity loss of lithium storage. Meanwhile, nitrogen doping not only modifies the electronic structure of the metal oxide owing to noticeably the improved electronic conductivity by narrowing the Nb_2O_5 bandgap, but also induces a pseudo-capacitance mechanism and increases the specific surface area of the material due to the generation of new phases.[23–26] Consequently, combining large-grain Nb_2O_5 nanowires with nitrogen doping can deliver attractive battery performance including high specific capacity and high rate ability.

Herein, we successfully prepare the high aspect ratio of ultrathin T–Nb_2O_5 nanowire by nitrogen doping with ammonia gas at different times (45 min, 90 min, and 120 min, respectively). The large grain T–Nb_2O_5 nanowires with nitrogen doping can form a conductive network on the surface to improve the material conductivity. Also, the structural defects caused by the micro-nitrogen doping can increase the lithium storage site and the pores on the material surface can increase the specific surface area, facilitating the rapid transportation of lithium-ion. Therefore, the N–T–Nb_2O_5 nanowire demonstrates superior electrochemical performance. In addition, it is the first

[a] *W. Fang, H. Zhang, L. Wu, E. Dong, G. Yin*
School of Chemistry, Baicheng Normal University, Zhongxingxi Street, Baicheng 137000, China
E-mail: ingeping@hit.edu.cn

[b] *L. Zhang*
College of Arts and Science, Northeast Agricultural University, Harbin 150030, China
E-mail: ingling20_05@163.com

[c] *M. Yang, X. Xiao, Y. Zhang, S. Lou, G. Yin*
State Key Laboratory of Space Power-Sources, School of Chemistry and Chemical Engineering, Harbin Institute of Technology, Harbin 150001, Heilongjiang, China

Supporting information for this article is available on the WWW under https://doi.org/10.1002/batt.202400065

time to find the nitriding process of T–Nb_2O_5 with ammonia gas and NbN with face-centered cubic crystal structure was synthesized in one step by high-temperature ammonolysis. Importantly, this work provides a new route to the reasonable design of anode materials for high-rate and long-cycling lithium-ion batteries.

Experimental Section

Preparation of T–Nb_2O_5 Nanowire

The T–Nb_2O_5 nanowire was prepared by a gentle hydrothermal synthesis of the Nb_2O_5 precursor and then high-temperature calcination at 600 °C. In detail, 0.26 g nano-niobium powder was added to 40 mL of NaOH solution (10 mol·L^{-1}) under stirring vigorously for 30 minutes. After the reaction, the obtained mixed solution was transferred to a 100 mL of Teflon-lined stainless steel autoclave and kept at 130 °C for 18 hours. The product was washed with deionized water 3 times and then soaked in dilute hydrochloric acid for 10 h. After that, the precursor can be obtained after freeze-drying. Finally, the precursor was calcined at 600 °C for 5 h with a heating rate of 5 °C min^{-1} in an air atmosphere to acquire the white T–Nb_2O_5 nanowire material.

Surface Nitriding Treatment of T–Nb_2O_5

The resulting T–Nb_2O_5 nanowire material was annealed at different times in the NH_3 atmosphere to achieve different degrees of nitriding of the material surface. The specific nitriding treatment process is as follows: the T–Nb_2O_5 nanowire material is heated until 600 °C with a heating rate of 10 °C/min at N_2 atmosphere. After that, the N_2 atmosphere is stopped and the NH_3 is introduced with 15 min, 30 min, 45 min, 60 min, 90 min, and 120 min, respectively. Finally, the samples with surface nitriding treatment of T–Nb_2O_5 were obtained and denoted as N–T–Nb_2O_5.

Characterization

The morphology and microstructure of the obtained samples were observed by the scanning electron microscope (FE-SEM, JEOL, S-4700) and the high-resolution transmission electron microscope (HRTEM, FEI, Tecnai G1F30). The intrinsic conductivity of N–T–Nb_2O_5 is performed by using the ultraviolet-visible light absorption spectrometer (UV-VIS, JEOL, UH4150). The phase information of the composites was characterized by an X'PERT type normal temperature/high temperature multifunctional X-ray diffractometer (XRD, Panalytical/Cu Kα radiation). Valence analysis of the obtained N–T–Nb_2O_5 sample was conducted by X-ray photoelectron spectroscopy (XPS, Kratos, AXIS ULTRA DLD).

Electrochemical Measurements

Electrochemical impedance spectroscopy (EIS) with a frequency range from 0.1 Hz to 10 kHz with an amplitude of 5 mV and cyclic voltammetry (CV) with a voltage from 1.0 to 3.0 V were determined by a CHI604d electrochemical workstation.

The electrochemical performance of the prepared sample material was tested by a CR2025 coin cell. The prepared active material, conductive material (Super P), and polyvinylidene fluoride (PVDF) binder are mixed in a mass ratio of 70%:20%:10%, and used as the working electrode. The mass loading of each electrode was about 1.5 mg cm^{-2}. For the coin cell assembly, a metal lithium disk is used as the counter electrode and $LiPF_6$ (1 mol/L) is dissolved in EC/DMC/DEC (1:1:1 vol) as the electrolyte. The LAND 2001CT analyzer was utilized to perform the charge/discharge tests in the range of 1.0~3.0 V at room temperature.

Constant Current Intermittent Titration Test

The chemical diffusion coefficient of lithium (D) is performed by the Galvanostatic intermittent titration technique (GITT) using 0.1 C constant current with a voltage range of 1.1–3.0 V, a pulse time of 12 min, and a relaxation time of 2 h.

2. Results and Discussion

In this work, a gentle hydrothermal synthesis approach has been employed to prepare T–Nb_2O_5 nanowires. As shown in **Figure S1**, It can be seen that after the precursor is calcined, the nanowires appear to be partially broken and agglomerated into bundles, and the products are nanowires with diameters of 200–500 nm and a large range of lengths, and the sample particles are larger. Figure 1a identified a smooth surface of T–Nb_2O_5 nanowires with a diameter of 200 to 500 nm, suggesting a small specific surface area. Also, the streaked nanowire surface further explains the layered structure of the T–Nb_2O_5 material. As presented in Figure 1b though there are no obvious changes in the diameter of 45N–T–Nb_2O_5 nanowires, more evenly distributed pores appear on the surface of nanowires, indicating the increased specific surface area after nitriding for 45 min. The many pores on the material surface can cause structural defects and further expose more lithium storage sites, improving the lithium storage capacity. Particularly, the amorphous regions on the particle surface (Figure 1c) are observed, which is speculated as the NbON layer (< 5 nm). The high-resolution TEM of 45N–T–Nb_2O_5 in Figure 1d exhibits clear lattice fringes with an interplanar spacing of 0.39 nm and 0.25 nm, corresponding to the (001) crystal plane of T–Nb_2O_5 and the (111) crystal plane of the NbN crystal, respectively.[27,28] Obviously, the polycrystals, as confirmed by the Fast Fourier Transform Results (FFT), indicate the formation of a new high electronic conductivity NbN crystal phase after nitrification for 45 min. Concurrently, it can be found that the Nb, O, and N of 1 D nanowires are very evenly distributed after surface nitriding with ammonia gas.

Furthermore, the overall morphology of 120N–T–Nb_2O_5 is unchanged compared to the T–Nb_2O_5 nanowires, while no representative lattice stripe and electron diffraction lattice of the (001) crystal plane were found (**Figure S2**), indicating that the T–Nb_2O_5 is completely transformed into a surface-cubic NbN after 120 min of nitride. Notably, for the first time, NbN with a cubic crystal structure can be prepared from T–Nb_2O_5 by a one-step process of high-temperature ammoniation.

To summarize, the nitride process is from the surface to the inside, with NbON acting as an intermediate product, gradually transforming into NbN crystals as the increased nitride proceeds. In addition, an increased conductive network and high specific surface area suggest that the pseudo-capacitive

Research Article
doi.org/10.1002/batt.202400065
Chemistry Europe
European Chemical Societies Publishing

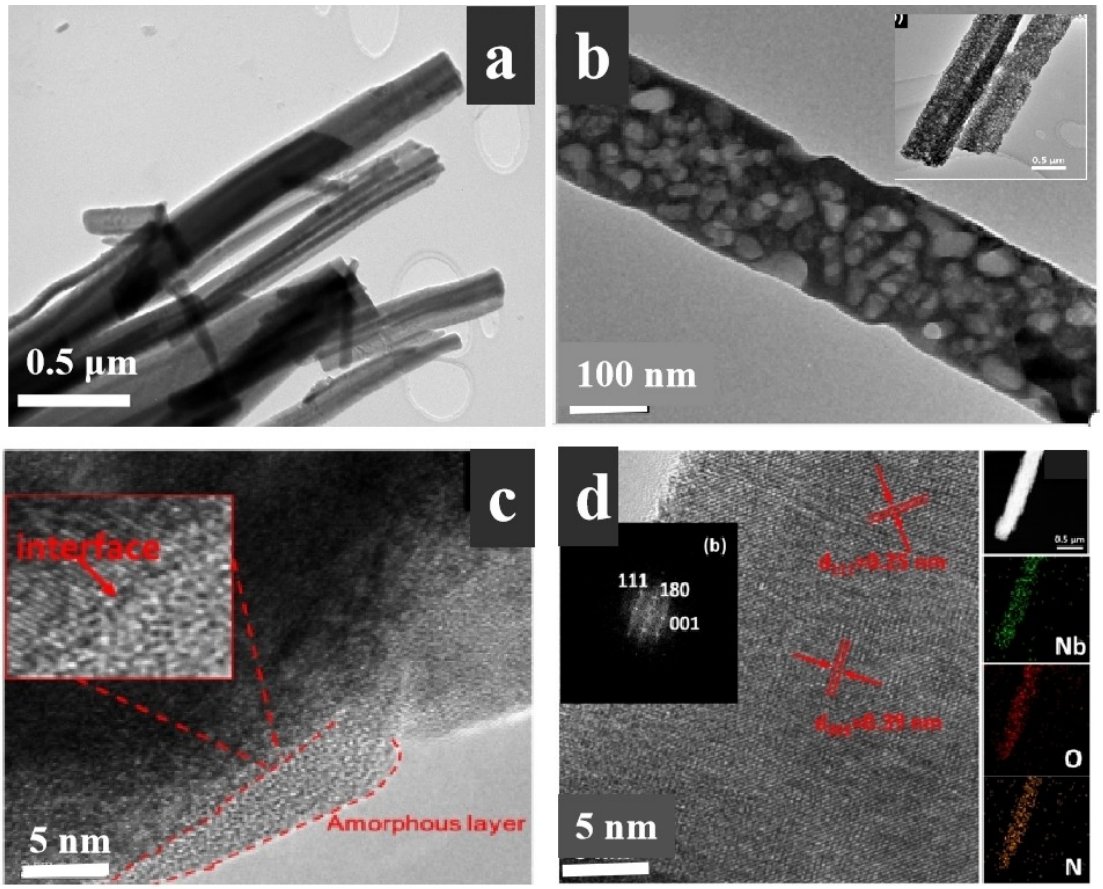

Figure 1. The high-resolution TEM image of T–Nb_2O_5 (a) and 45N–T–Nb_2O_5 (b, c), and the corresponding FFT and elemental mapping images of 45N–T–Nb_2O_5(d).

effect can be fully utilized, improving the rate performance of the N–T–Nb_2O_5 material.

All XRD diffraction peaks of the obtained T–Nb_2O_5 and N–T–Nb_2O_5 (Figure 2a) can be well attributed to the orthorhombic (T) phase (JPCDS. No. #27-1003).[29] Since the color of the material gradually changes from pure white to gray, then to dark gray, and eventually to black with the prolongation of the nitride time, the nitride degree of T–Nb_2O_5 nanowire materials can also be easily distinguished from the product color. The diffraction peak intensity of T–Nb_2O_5 was gradually weakened and widened with prolonged nitride time, which may be related to the introduction of the NbON amorphous layer in the material surface during the process of nitride. When the nitride time was up to 120 min, the T–Nb_2O_5 diffraction peak basically disappeared and that of the NbN crystal appeared, so the nitride time need to be strictly controlled.

As can be seen in Figure 2b, the UV electromagnetic wave absorption is reduced as increased nitriding time, especially the 90 min, indicating that the deepening of N incorporation improves the conductivity of T–Nb_2O_5, thus benefiting the lithium-ion battery's high rate capacity. The XPS test was performed to analyze the element valence of N–T–Nb_2O_5 and the result is shown in Figure 2c–**e**. In Nb3d spectra (Figure 2c), the peaks at 207.0 eV, 204.2 eV, and 203.2 eV, are ascribed to the Nb^{5+}–O, Nb^{5+}–N, and Nb^{3+}–N, respectively, indicating that the surface of 90-N–T–Nb_2O_5 is still mainly Nb_2O_5, with only small amounts of NbON and NbN.[29,30] The N1s spectra can be fitted into two peaks, consistent with the N–Nb at 396.4 eV and N–O–Nb at 402.2 eV (Figure 2d).[31] The O1s spectrum displays three fitting peaks (Figure 2e), which correspond to Nb–O (206.9 eV), Nb–O–N (531.3 eV), and O–H (532.5 eV), respectively.[32]

Therefore, combining the results of the above analysis, the nitridation of the T–Nb_2O_5 material is gradually deepened from the surface to the inside, and the NbON is in an intermediate state. Also, it is eventually converted to NbN as the deepened nitridation degrees.

There is no obvious voltage platform in the charge/discharge curves in Figure 3a, indicating that the pseudocapacitive effect of T–Nb_2O_5 is not reduced or eliminated after nitridation, namely, N–T–Nb_2O_5 is also a typical pseudocapacitors material. The cycling performances of N–T–Nb_2O_5 at 0.1 C, 0.5 C, and 10 C are shown in Figure 3b–**d**. The initial charging specific capacity of 45N–T–Nb_2O_5 at 0.1 C can reach 238.3 mAh g^{-1}, higher than the theoretical specific capacity (201.6 mAh g^{-1}), which may be associated with the fact that the material surface has more cation sites and larger specific surface area of NbON amorphous thin layer after nitrogen doping. It

Research Article
doi.org/10.1002/batt.202400065
Chemistry Europe
European Chemical Societies Publishing

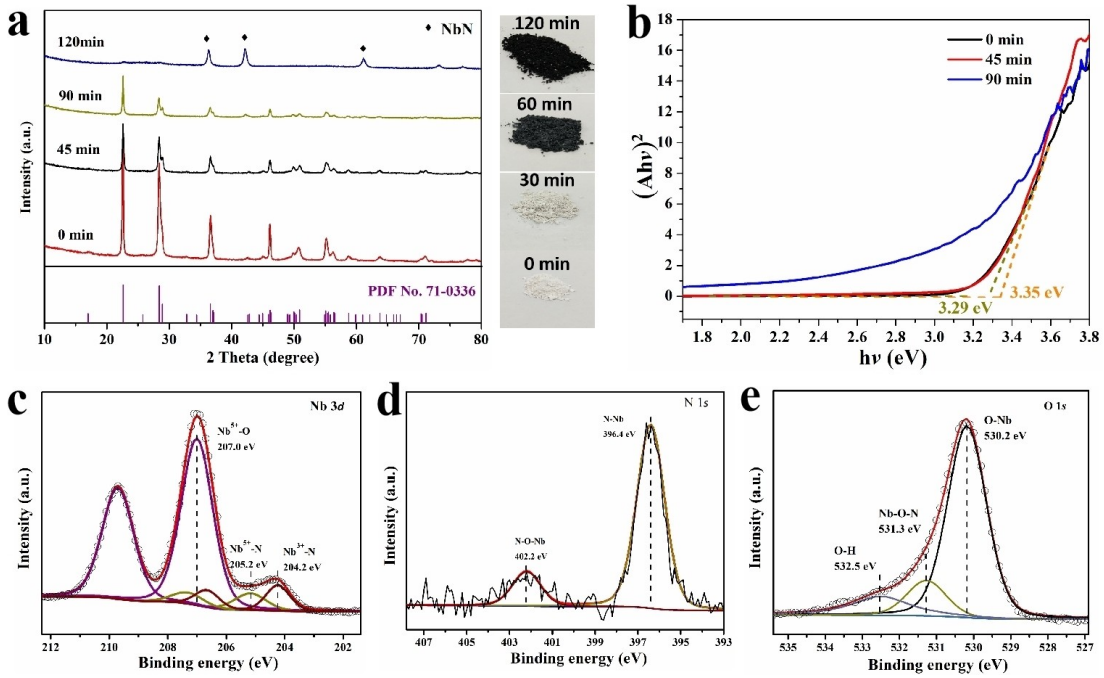

Figure 2. (a) The XRD patterns, (b) band gap width of T–Nb_2O_5 subjecting nitrification at different times, and XPS spectra of 90N–T–Nb_2O_5: (c) Nb 3d, (d) N 1s and (e) O1s.

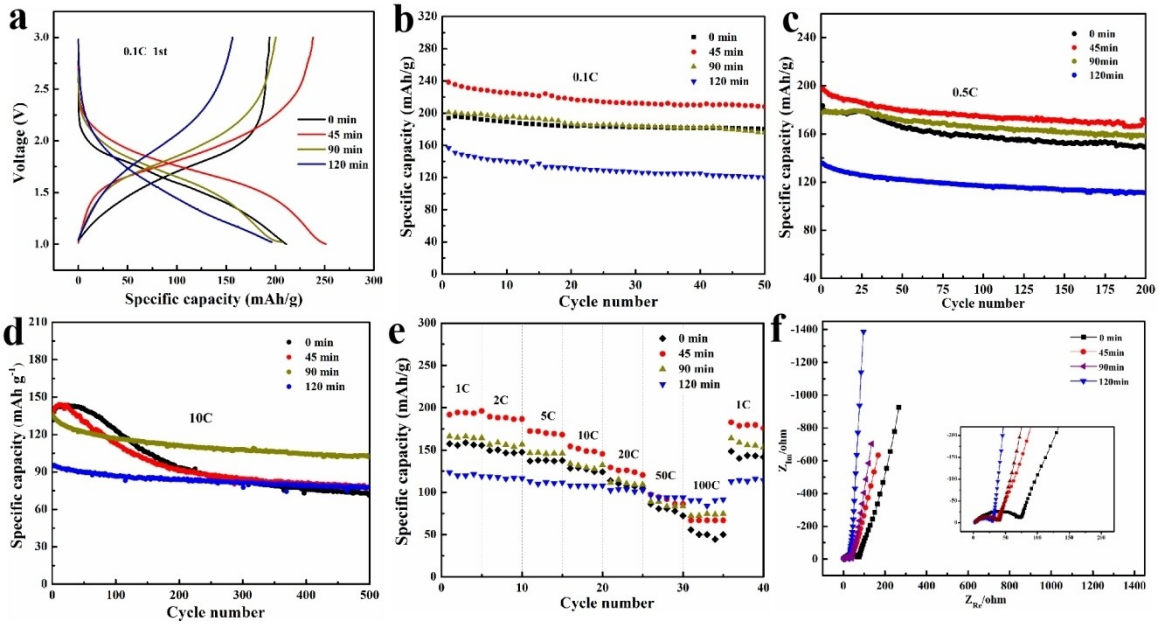

Figure 3. (a) charging/discharging curves, (b–d) cycling performances at 0.1 C, 0.5 C and 10 C, respectively, (e)rate performances, (f) EIS spectra of the N–T–Nb_2O_5 at different time.

can be found that the T–Nb_2O_5 subjecting nitridation does not exhibit their cycling advantages than that of pure T–Nb_2O_5 at a low rate (0.1 C and 0.5 C), which may be related to the fact that the process of lithium-ion intercalation/de-intercalation is relatively moderate and less destructive to the material structure at a low rate. However, from Figure 3d, after 500 cycles at 10 C, the capacity retention rate of T–Nb_2O_5, 45N–T–Nb_2O_5, 90N–T–Nb_2O_5, and the 120N–T–Nb_2O_5 was 53.0%, 57.3%, 75.2%, and 81.3%, respectively, indicating that the cycle stability of T–Nb_2O_5 is improved at a higher rate with the deepening of the nitride degree. This may be related to the thickening and increasing pores of the nitride layer on the material surface, which can effectively buffer against volume expansion and optimize mechanical properties.[27] Yet the initial capacity decrease of 120N–T–Nb_2O_5 is related to the lack of lithium storage sites in NbN itself.

Research Article
doi.org/10.1002/batt.202400065
Chemistry Europe
European Chemical Societies Publishing

The rate performance of the N–T–Nb_2O_5 materials in the potential range of 1.0–3.0 V was also evaluated, as shown in Figure 3e. With the increase of the nitrogen degree, the specific capacity increases first and then decreases at a lower rate, which is related to the lack of lithium storage sites owing to the changed surface from NbON to NbN. However, when the rate reaches 50 C and 100 C, the high rate performance is improved as the deepening nitrification degree. Since the increased conductor properties of T–Nb_2O_5 materials are due to deepened nitrification, the transmission rate of the electron is accelerated. Also, the pores on the material surface and the generated NbON amorphous layer increase the contact area of the electrode material and the electrolyte, shortening the transmission path of lithium ions, as confirmed by the SEM and TEM. Therefore, the deeper the nitrification degree, the better the high-rate performance of the N–T–Nb_2O_5 material.

Compared with pure T–Nb_2O_5, the charge-transfer resistance (*R*ct) value is reduced significantly as increased nitridation degrees (Figure 3f), indicating that N–T–Nb_2O_5 materials are more beneficial to electrochemical reactions.[33] Meanwhile, the linear inclination angle of the T–Nb_2O_5 is also increased with deepened nitridation degrees, presenting the pseudocapacitance characteristics of T–Nb_2O_5. It is worthwhile to note that the 120N–T–Nb_2O_5 is even close to 90 degrees, indicating that the nitridation can exert a more significant pseudocapacitance effect during lithium intercalation/deintercalation. Moreover, the technology of constant current intermittent titration (GITT) is performed to study the influence of the lithium-ion diffusion coefficient of material (**Figure S3**). The simplified formula[27] based on Fick's second law is used for the diffusion coefficient of lithium-ion.

$$D = \frac{4}{\pi\tau}\left(\frac{n_B V_M}{S}\right)^2 \left(\frac{\Delta E_S}{\Delta E_\tau}\right)^2$$

Where τ is the pulse time, n_B is the molar number of the active substance, V_M is the molar volume of the active material, S is the electrode/electrolyte contact area, $\triangle Es$ is the steady-state potential difference, and $\triangle E\tau$ is the potential difference caused by the pulse current. It can be seen that under different lithium intercalated amounts $(D_{Li+})_{N-T}/(D_{Li+})_T$ is close to 1 as a whole while the ratio is greater than 1 at the lithium intercalated amount $x < 0.3$, proving that the advantages of high specific surface area can be full utilization in the state of low lithium intercalated amount and the smooth ion transport channel inside the material.

To determine the relationship between the electrochemical rapid lithium intercalated characteristics and the pseudocapacitance of T–Nb_2O_5 material, the CV is performed in the potential window of 1.0~3.0 V (*vs* Li^+/Li). As presented in Figure 4a–**c** that

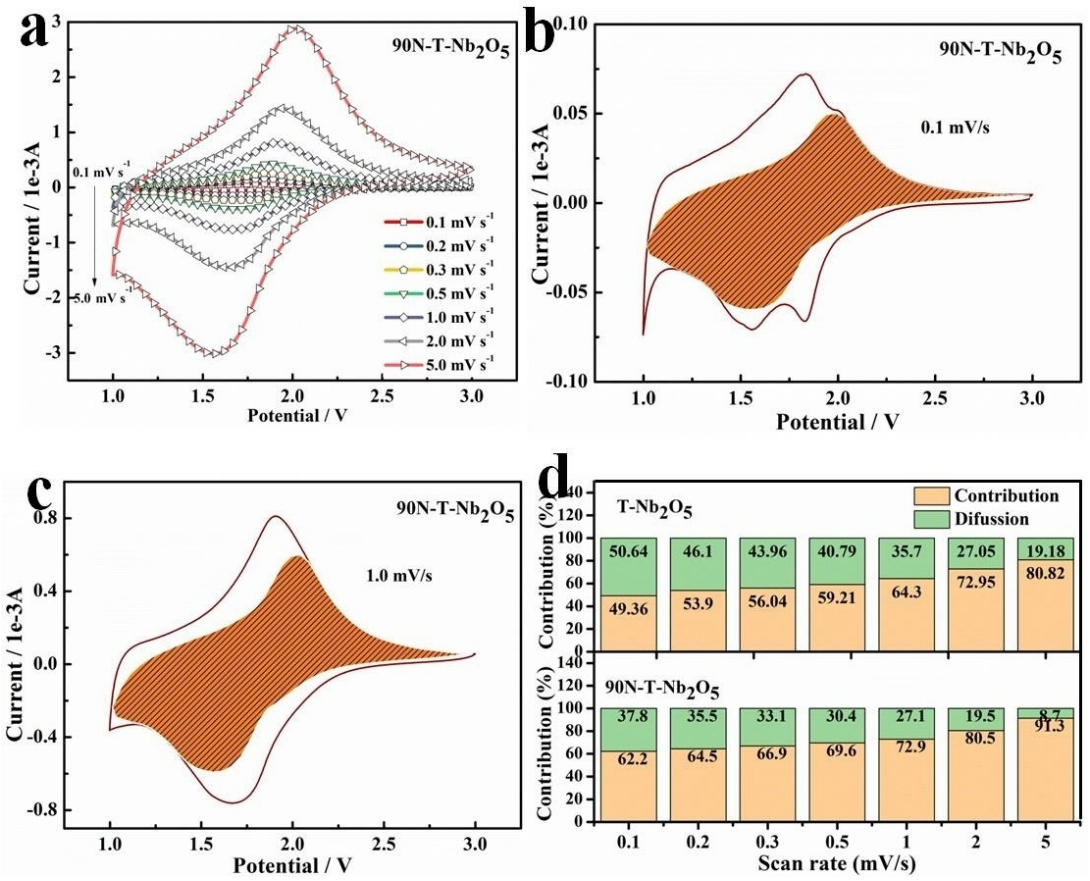

Figure 4. (a) CV curves at different scan rates of 90N–T–Nb_2O_5, the proportion of the capacitance current (shaded region) at the scan rate of 0.1 mV s^{-1} (b) and 1.0 mV s^{-1} (c) for 90N–T–Nb_2O_5, and (d) the contribution ratio of capacitive capacities and diffusion capacity of T–Nb_2O_5 and 90N–T–Nb_2O_5.

both the oxidation and the reduction peak are the "steamed bread" peaks, and the voltage separations are very small, reflecting the typical electrochemical characteristics of the pseudocapacitance materials. For T–Nb_2O_5, the ratio of oxidation peak and reduction peak (I_{Pa}/I_{Pc}) gradually decreases (**Table S1**), while the I_{Pa}/I_{Pc} of 90N–T–Nb_2O_5 is closer to 1 or greater than 1 (**Table S2**), indicating that the electrochemical reversibility of 90N–T–Nb_2O_5 at a high rate is better than T–Nb_2O_5, as confirmed by the rate performance.

Moreover, the relationship between peak current and the scan rate of the CV curve is studied in Equation 2, and the result is shown in **Figure S4**.

$$i = av^b \quad (2)$$

Where i is the peak current (A) of the oxidation/reduction reaction at different scan rates, and v is the corresponding scan rate (mV s^{-1}). a and b are correlation coefficients, which can be determined from the linear fitting of the Log (i) vs. Log(v) through Equation[35–37] (3):

$$\mathrm{Log}(i) = b\mathrm{Log}(v) + \mathrm{Log}(a) \quad (3)$$

The value of b reflects the main control process of electrode reaction. It can be found that the b-value for both T–Nb_2O_5 (0.87 and 0.84) and 90N–T–Nb_2O_5 (0.97 and 0.93) is close to 1, especially 90N–T–Nb_2O_5, indicating that the pseudocapacitance effect of nitride materials is more obvious. At the same time, the b value of the reduction process is slightly greater than that of the oxidation process, which proves that the intercalation dynamics of lithium ions are better than the deintercalation dynamics.

The capacity contributions of the diffusion and pseudocapacitance control process are calculated by Equation (4).[38,39]

$$i(\mathrm{V}) = k_1 v + k_2 v^{1/2} \quad (4)$$

Where i (V) is the total current (A) at a given potential, $k_1 v$ and $k_2 v^{1/2}$ represent the current of the pseudocapacitance and diffusion control process, respectively. The values of k_1 and k_2 can be acquired by fitting the curve of i (V)/$v^{1/2}$ to $v^{1/2}$ at a specific potential, the slope and intercept, respectively. The capacity contribution of pseudocapacitance and diffusion at 0.1 mV/s and 1.0 mV/s can are shown in Figure 4d. It can be found that the proportion of the pseudocapacitance contribution is larger for 90N–T–Nb_2O_5 compared with that of T–Nb_2O_5, indicating the higher pseudocapacitance after nitriding. Obviously, in rapid charging and discharging processes, the excellent rate performance of the 90N–T–Nb_2O_5 material almost all comes from the pseudocapacitive efficiency. Moreover, since the pseudogenic effect is a rapid Faraday reaction occurring on the material surface or near the surface, without causing the phase transition and structural damage of the material, the electrochemical performance of T–Nb_2O_5 material is improved after nitrogen-doping with ammonia.

3. Conclusions

In this work, the high stability of T–Nb_2O_5 nanowires with more evenly distributed pores were synthesized by surface nitrogenated with ammonia. For the first time, the nitriding process with ammonia was found to be from the surface to the interior, and NbON, as an intermediate product, is gradually transformed into NbN with the face-centered cubic crystal structure. Therefore, the NbN can be firstly synthesized from T–Nb_2O_5 by ammonolysis at high temperatures in one step. Among them, the first reversible specific capacity of 45N–T–Nb_2O_5 at 0.1 C is 238.33 mAh g^{-1}, higher than that of the theoretical specific capacity, which is related to the structural defects caused by the excess cation sites and pores caused by nitrogen doping. With the deepening of nitride degree on the surface of the T–Nb_2O_5 material, the specific surface area is increased, the electrical conductivity is enhanced, and the rate performance is also improved due to porous structure after surface nitridation treatment.

The pseudocapacitance effect of T–Nb_2O_5 and N–T–Nb_2O_5 plays a decisive role in the high rate capacity, and the proportion of the capacity controlled by the pseudocapacitance is increased with the increasing rate, indicating that the capacity at high rates is mainly controlled by the pseudocapacitance effect. Meanwhile, with the deepening of the surface nitriding degree, the pseudo-capacitance effect becomes more obvious and the N–T–Nb_2O_5 show better rate performance, which is related to better conductivity and higher specific surface area after surface nitridation.

Acknowledgements

This work was supported by the Natural Science Foundation of Heilongjiang Province (No. LH2021B004), the National Natural Science Foundation of China (No. 22209022), the Jilin Provincial Development and Reform Commission (No. 2023C034-1) and the Jilin Provincial Department of Education project China (No. JJKH20230017KJ).

Conflict of Interests

The authors declare no conflict of interest.

Data Availability Statement

Research data are not shared.

Keywords: Lithium-ion batteries · T–Nb_2O_5 · Surface nitrogen doping · High-rate capability · Pseudocapacitive effect

[1] J. L. Li, J. Fleetwood, W. B. Hawley, *Chem. Rev.* **2022**, *122*, 903–956.
[2] Q. Meng, C. Kang, J. M. Zhu, X. J. Xiao, Y. L. Ma, H. Huo, P. J. Zuo, C. Y. Du, S. F. Lou, G. P. Yin, *Nano Lett.* **2022**, *22*, 5553.

[3] S. Lou, Q. Liu, F. Zhang, Q. Liu, Z. Yu, T. Mu, Y. Zhao, J. Borovilas, Y. Chen, M. Ge, X. Xiao, W.-K. Lee, G. Yin, Y. Yang, X. Sun, *Nat. Commun.* **2020**, *11*, 5700.
[4] Q. Meng, J. M. Zhu, C. Kang, X. J. Xiao, Y. L. Ma, H. Huo, P. J. Zuo, C. Y. Du, S. F. Lou, *Small.* **2022**, *18*, 2204745.
[5] T. T. Li, K. T. Liu, G. Nam, M. G. Kim, Y. Ding, B. T. Zhao, Z. Y. Luo, Z. R. Wang, W. L. Zhang, C. X. Zhao, J. H. Wang, Y. Y. Song, *Small.* **2022**, *18*: 2200972.
[6] F. Shen, Z. T. Sun, L. Zhao, Y. H. Xia, Y. Y. Shao, J. S. Cai, S. Li, C. Lu, X. L. Tong, Y. Zhao, J. Y. Sun, *J. Mater. Chem. A.* **2021**, *9*, 14534–14544.
[7] T. T. Li, G. Nam, K. T. Liu, J. H. Wang, B. T. Zhao, Y. Ding, L. K. Soule, M. Avdeev, Z. Y. Luo, *Adv. Energy Mater.* **2021**, *15*: 254–264.
[8] Y. Zhang, C. Kang, W. Zhao, B. Y. Sun, X. J. Xiao, H. Huo, Y. L. Ma, P. J. Zuo, S. F. Lou, *Energy Storage Mater.* **2022**, *47*, 178–186.
[9] J. Meng, Q. He, L. Xu, X. Zhang, F. Liu, X. Wang, Q. Li, X. Xu, G. Zhang, C. Niu, *Adv. Energy Mater.* **2019**, *9*, 1802695.
[10] W. Fang, Y. Zhang, C. Kang, Q. Meng, A. R. Shi, S. F. Lou, X. Q. Cheng, G. P. Yin, *Appl. Surf. Sci.* **2022**, *600*, 154068.
[11] V. Augustyn, J. Come, M. A. Lowe, J. W. Kim, P. L. Taberna, S. H. Tolbert, H. D. Abruña, P. Simon, B. Dunn, *Nat. Mater.* **2013**, *12*, 518.
[12] S. F. Lou, Y. Zhao, J. J. Wang, G. P. Yin, C. Y. Du, X. L. Sun, *Small.* **2019**, *15*, 1904740.
[13] X. Wang, G. Li, Z. Chen, V. Augustyn, X. Ma, G. Wang, B. Dunn, Y. Lu, *Adv. Energy Mater.* **2011**, *1*, 1089–1093.
[14] V. Augustyn, P. Simon, *Energy Environ. Sci.* **2014**, *7*, 1597–1609.
[15] S. Lou, F. Zhang, C. Fu, M. Chen, Y. Ma, G. Yin, J. Wang, *Adv. Mater.* **2021**, *33*, 2000721.
[16] D. Cao, Z. Yao, J. Liu, J. Zhang, *Energy Storage Mater.* **2018**, *11*, 152–160.
[17] X. Han, Q. Meng, X. Wan, B. Y. Sun, Y. Zhang, B. C. Shen, J. L. Gao, Y. L. Ma, P. J. Zuo, S. F. Lou, *Nano Energy.* **2021**, *81*, 105635.
[18] H. R. Li, D. Li, J. Shi, Z. Y. He, Z. C. Zhao, *Sustain. Energy Fuels* **2020**, *4*, 4868–4877.
[19] J. S. Meng, Q. He, L. H. Xu, X. C. Zhang, F. Liu, X. P. Wang, Q. Li, X. M. Xu, G. B. Zhang, C. J. Niu, Z. T. Xiao, Z. Liu, Z. Z. Zhu, Y. Zhao, *Adv. Energy Mater.* **2019**, *9*, 1802695.
[20] S. F. Lou, X. Q. Cheng, Y. Zhao, Lushington, A. J. L. Gao, Q. Li, P. J. Zuo, B. Q. Wang, Y. Z. Gao, Y. L. Ma, C. Y. Du, G. P. Yin, *Nano Energy.* **2017**, *34*, 15–25.
[21] Y. Lei, S. Jie, C. Xing, H. Zhu, H. Yu, C. Zhang, Z. Yang, X. Ying, Z. Guo, *Energy Storage Mater.* **2018**, *16*, 535–544.
[22] X. Cai, H. Yan, R. Zheng, H. Yu, Z. Yang, X. Zhang, M. Xia, W. Chen, Y. Cui, *Inorg. Chem. Front.* **2020**, *8*, 444–451.
[23] H. Park, H. B. Wu, T. Song, *Adv. Energy Mater.* **2015**, *5*, 1401945.
[24] X. Wang, X. Yuan, D. Wang, et al., *ACS Appl. Energ. Mater.* **2018**, *1*, 876–882.
[25] S. Hemmati, G. Li, X. L. Wang, Y. L. Ding, Y. Pei, A. P. Yu, *Nano Energy.* **2019**, *56*, 118–126.
[26] Z. P. Jin, Z. Cai, X. S. Chen, Nano Res. **2018**, *11*, 8–16.
[27] Y. J. Zheng, Z. G. Yao, Z, P. Shadike, M. Lei, J. J. Liu, *Adv. Funct. Mater.* **2022**, *32*, 2107060.
[28] D. Wang, Z. H. Zhang, D. X. Zhang a, Z. C. Zheng, G. Chen, N. Zhang, X. H. Liu, R. Z. Ma, *J. Power Sources.* **2022**, *530*, 231274.
[29] J. Yu, Z. Chen, L. Zeng, Y. Ma, Z. Feng, Y. Wu, H. Lin, L. Zhao, Y. He, *Sol. Energy Mater. Sol. Cells* **2018**, *179*, 45–56.
[30] Q. Deng, M. Li, J. Wang, P. Zhang, K. Jiang, J. Zhang, Z. Hu, J. Chu, *Sci. Rep.* **2017**, *7*, 1883.
[31] V. V. Atuchin, I. E. Kalabin, V. G. Kesler, N. V. Pervukhina, *J. Electron Spectrosc. Relat. Phenom.* **2005**, *142*, 129–134.
[32] Y. Lian, Y. Zheng, Y. Bai, D. Wang, H. Yan, Z. Wang, J. Zhao, H. Zhang, *J. Power Sources.* **2021**, *507*, 230267.
[33] Y. Lian, D. W. Wang, S. Y. Hou, C. L. Ban, J. Zhao, H. H. Zhang, *Electrochim. Acta* **2019**, *330*, 135204.
[34] V. Augustyn, J. Come, M. A. Lowe, J. W. Kim, P. L. Taberna, S. H. Tolbert, H. D. Abruna, P. Simon, B. Dunn, *Nat. Mater.* **2013**, *12*, 518–522.
[35] H. Lindström, S. Södergren, A. Solbrand, H. Rensmo, J. Hjelm, A. Hagfeldt, S. E. Lindquist, *J. Phys. Chem. B* **1997**, *101*, 7717–7722.
[36] G. Y. Liu, S. S. Liu, H. Chen, X. D. Liu, X. W. Luo, X. Li, J. M. Ma, *Nanoscale.* **2022**, *14*, 11710–11718.
[37] P. Simon, Y. Gogotsi, B. Dunn, *Science.* **2014**, *343*, 1210–1211.
[38] V. Augustyn, J. Come, M. A. Lowe, J. W. Kim, P. L. Taberna, S. H. Tolbert, H. D. Abruna, P. Simon, B. Dunn, *Nat. Mater.* **2013**, *12*, 518–522.
[39] J. Tian, D. Cao, X. Zhou, J. Hu, M. Huang, C. Li, *ACS Nano.* **2018**, *12*, 3424–3435.

Manuscript received: January 30, 2024
Revised manuscript received: February 24, 2024
Accepted manuscript online: March 7, 2024
Version of record online: April 11, 2024